Potent anti-tumor effects of receptor-retargeted syncytial oncolytic herpes simplex virus

Takuma Suzuki,[1,2] Hiroaki Uchida,[1] Tomoko Shibata,[1] Yasuhiko Sasaki,[1] Hitomi Ikeda,[1] Mika Hamada-Uematsu,[1] Ryota Hamasaki,[1,3] Kosaku Okuda,[1,3] Shigeru Yanagi,[2] and Hideaki Tahara[1,4]

[1]Project Division of Cancer Biomolecular Therapy, The Institute of Medical Science, The University of Tokyo, 4-6-1 Shirokanedai, Minato-ku, Tokyo 108-8639, Japan; [2]Laboratory of Molecular Biochemistry, School of Life Sciences, Tokyo University of Pharmacy and Life Sciences, Tokyo, Japan; [3]Ono Pharmaceutical Co., Ltd., Osaka, Japan; [4]Department of Cancer Drug Discovery and Development, Osaka International Cancer Institute, Osaka, Japan

Most oncolytic virotherapy has thus far employed viruses deficient in genes essential for replication in normal cells but not in cancer cells. Intra-tumoral injection of such viruses has resulted in clinically significant anti-tumor effects on the lesions in the vicinity of the injection sites but not on distant visceral metastases. To overcome this limitation, we have developed a receptor-retargeted oncolytic herpes simplex virus employing a single-chain antibody for targeting tumor-associated antigens (RR-oHSV) and its modified version with additional mutations conferring syncytium formation (RRsyn-oHSV). We previously showed that RRsyn-oHSV exhibits preserved antigen specificity and an ~20-fold higher tumoricidal potency in vitro relative to RR-oHSV. Here, we investigated the in vivo anti-tumor effects of RRsyn-oHSV using human cancer xenografts in immunodeficient mice. With only a single intra-tumoral injection of RRsyn-oHSV at very low doses, all treated tumors regressed completely. Furthermore, intravenous administration of RRsyn-oHSV resulted in robust anti-tumor effects even against large tumors. We found that these potent anti-tumor effects of RRsyn-oHSV may be associated with the formation of long-lasting tumor cell syncytia not containing non-cancerous cells that appear to trigger death of the syncytia. These results strongly suggest that cancer patients with distant metastases could be effectively treated with our RRsyn-oHSV.

INTRODUCTION

Oncolytic virotherapy using herpes simplex virus type 1 (HSV-1) is showing promise as a novel cancer therapy.[1,2] To date, multiple clinical trials have utilized genetically modified oncolytic HSVs (oHSVs) that are deficient in viral genes essential for replication in normal cells but not in cancer cells.[3–5] These include the genes encoding infected cell polypeptide (ICP)34.5, a major determinant of HSV neurovirulence that inhibits the cellular protein kinase R (PKR) that blocks viral replication in normal cells.[6,7] However, PKR responses are commonly impaired in tumor cells.[8] Thus, HSV-1 can replicate selectively in tumor cells even without functional ICP34.5 genes. Clinical trials have shown that these types of oHSVs, henceforth termed "conditionally replicating oHSVs" (CR-oHSVs), can be safely administered to humans.[3–5] Among the clinically developed CR-oHSVs, talimogene laherparepvec (T-VEC) was recently approved for clinical use in the United States and the European Union for melanoma patients.[5,9,10] However, the route of administration of CR-oHSVs in the majority of clinical trials has been by direct injection into the tumor,[3–5] since the CR-oHSVs are not ideal for systemic administration, at least partially because they might be sequestered by a wide variety of normal cells that also express HSV entry receptors. This may limit the therapeutic potential of CR-oHSVs, especially against metastatic tumor deposits that cannot be easily accessed, or even detected. Indeed, a phase III clinical trial showed that overall survival of patients treated by intra-tumoral injection of T-VEC was significantly better than the survival of patients treated with granulocyte-macrophage colony-stimulating factor (GM-CSF) (control arm) but only in a subgroup analysis of patients without distant visceral metastases.[5,9,10] Furthermore, preclinical studies on CR-oHSVs by different groups demonstrated that viral replication can be significantly hampered in certain types of tumor cells depending on the deleted HSV genes, and various strategies to address this limitation have been reported.[11–14] Thus, there is significant room for improvements in the development of CR-oHSV for clinical application.

In order to circumvent these problems with CR-oHSV, several groups including ours have developed a distinct class of oHSV, referred to here as "receptor-retargeted oHSV" (RR-oHSV), which can specifically enter cells expressing the target molecules on the cell surface. Zhou and Roizman were the first to show that this approach is feasible.[15] They genetically engineered the envelope glycoprotein D (gD) of HSV to bind not to its natural receptors on host cells (either
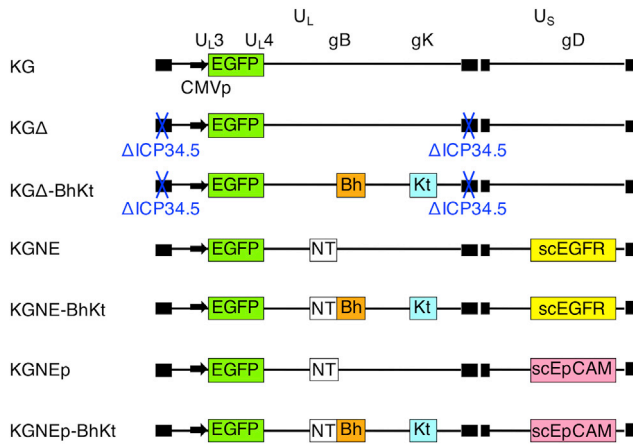
Figure 1. Schematic representation of the genomic structures of the recombinant HSVs used in this study

U_L, unique long segment; U_S, unique short segment; CMVp, human cytomegalovirus major immediate-early (HCMV-IE) promoter; EGFP, expression cassette for EGFP inserted in the intergenic region between the UL3 and UL4 genes; ΔICP34.5, deletion of ICP34.5 gene; Bh, R858H mutation in gB; Kt, A40T mutation in gK; NT, D285N/A549T mutations in gB that increase the rate of virus entry; scEGFR, anti-hEGFR scFv-fused gD; scEpCAM, anti-hEpCAM scFv-fused gD; Closed boxes, terminal and internal inverted repeats.

herpesvirus entry mediator [HVEM], nectin-1, or 3-O-sulfated heparan sulfate [3-OS-HS][16–18]) but to interleukin (IL)-13 receptors via the IL-13 incorporated into the gD. The mutant HSV was shown to selectively infect only cells bearing IL-13 receptors.[15] Furthermore, Menotti and colleagues showed that target-specific entry could be also achieved with the gD engineered to have a single-chain antibody (scFv) that binds to the target molecules on the cell membrane.[19] We also have developed a different RR-oHSV platform that can specifically and efficiently infect the target cells. In our construct, residues 2–24 in the HVEM-binding region of gD were deleted to impair binding to both HVEM and 3-OS-HS,[20] and a single amino acid substitution (Y38C) was made in gD to ablate binding to nectin-1.[21,22] We then inserted an scFv at the site of the deleted HVEM-binding residues. Furthermore, to enable efficient antigen-specific entry, we also employed the entry-enhancing mutations we had previously identified in glycoprotein B (gB) (D285N/A549T).[23] We have shown that our construct works well with a variety of different scFvs binding to tumor-associated antigens including human epidermal growth factor receptor (hEGFR), carcinoembryonic antigen, or epithelial cell adhesion molecule (hEpCAM).[21,22] Such RR-oHSVs enter cancer cells in an antigen-specific manner and are able to spread without losing their specificity for the cognate target antigen. Moreover, they exhibited significant anti-tumor effects both *in vitro* and *in vivo*.[21,22]

Using our RR-oHSV platform, we have sought to develop constructs with more robust anti-tumor effects by focusing on the properties of membrane fusion, which is the key process for both initial cell entry and subsequent lateral spread of HSV.[24] Cell-to-cell spreading of

HSV-1 typically occurs through release of progeny virions into spaces between infected cells and the surrounding uninfected cells *in vitro*. Infected cells become rounded and aggregate together, but with limited cell-cell fusion. However, certain HSV mutants can spread to surrounding cells by mediating fusion between the infected cell and adjacent uninfected cells.[25,26] This frequently leads to the formation of multinucleated giant cells, termed syncytia. Most of the mutations responsible for this hyperfusogenic phenotype, referred to as syncytial mutations, have been identified as single point mutations in the gB or gK genes.[25,26] Several groups have sought to confer such hyperfusogenic phenotypes upon CR-oHSVs in order to improve their anti-tumor efficacy.[27–30] For our RR-oHSVs, we introduced syncytial mutations into the gB and gK genes of the RR-oHSVs specific for hEGFR or hEpCAM and found that each of these recombinant viruses, termed RRsyn-oHSVs, caused the development of syncytia and had an ∼20-fold increased *in vitro* cytotoxicity for cancer cells expressing the cognate retargeted receptor.[24] However, the characteristics and magnitude of the *in vivo* anti-tumor effects of RRsyn-oHSV remain to be directly compared to those of the original non-syncytial RR-oHSV, CR-oHSV, or CR-oHSV with the same syncytial mutations (CRsyn-oHSV).

In the present study, we address this question using human tumor xenograft models in mice that are treated with intra-tumoral or intra-venous injection of these oHSVs. The findings of the study imply that clinical development of RRsyn-oHSVs might be beneficial for cancer patients.

RESULTS

Intra-tumoral injection of either an hEGFR-specific RR-oHSV or an ICP34.5-deleted CR-oHSV results in significant anti-tumor effects in a human tumor xenograft model in mice

We first examined the anti-tumor effects of KGNE,[21,22] an RR-oHSV specific for hEGFR, and KGΔ (a CR-oHSV similar to a well-characterized agent, HSV1716,[3] that has deletions of both copies of ICP34.5) (Figure 1). The anti-hEGFR scFv used here does not bind to the murine EGFR and thus provides an optimal model for an RR-oHSV that can enter only into cancer cells, but not non-cancerous cells, in immunodeficient mice bearing human tumors. We tested these two oHSVs using subcutaneous U87 xenografts that have often been employed for the assessment of the anti-tumor effects of oHSVs in multiple studies, including those for T-VEC and G47Δ that have recently been approved for clinical use.[12,31] Thus, we treated subcutaneous U87 tumors (tumor size ∼310 mm³) with a single intra-tumoral injection of PBS or either 10^4 or 10^7 pfu of each of the two oHSVs, KGNE and KGΔ. As shown in Figure 2, PBS-injected tumors increased in size and grew to >2,000 mm³ over a period of 21 days after injection, whereas the growth of tumors injected with 10^7 pfu of KGNE was suppressed during the first 9 days. This resulted in only a limited increase in size at the end of the observation period (p < 0.0001, compared to PBS). Although less marked (p < 0.0001, compared to 10^7 pfu), injection of 10^4 pfu of KGNE also significantly delayed the growth of tumors relative to the PBS control (p < 0.0001). In contrast, injection of
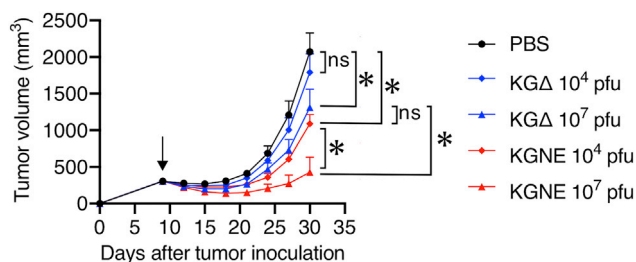
Figure 2. Efficiency of anti-tumor activity of a single intra-tumoral injection of hEGFR-specific RR-oHSV and ICP34.5-deleted CR-oHSV

U87 cells were injected subcutaneously into SCID-beige mice. When tumor volumes reached ~310 mm^3 (arrow), PBS (black circles; n = 6), 10^4 (blue diamonds; n = 6) or 10^7 (blue triangles; n = 6) pfu of KGΔ, or 10^4 (red diamonds; n = 6) or 10^7 (red triangles; n = 6) pfu of KGNE was injected into the tumors. Tumor volumes were measured, and mean volumes ± standard errors (SEs) are shown. Two-way repeated-measures analysis of variance (ANOVA) was used for comparative analysis. *p < 0.05; ns, not significant. Experiments were repeated twice, and similar results were observed.

10^4 pfu of KGΔ failed to affect growth of the tumors, which remained similar to the PBS control (p = 0.77) (Figure 2). Furthermore, although injection of 10^7 pfu of KGΔ did significantly delay the growth of tumors relative to PBS injection (p < 0.001), the effect was much less than the same dose of KGNE (p < 0.0001) and was similar to 10^4 pfu of KGNE (i.e., a 1,000-fold lower dose) (p = 0.43) (Figure 2). These results suggest that KGNE is a potent oHSV that mediates significant anti-tumor effects even at a dose lower than KGΔ. We also injected KG (Figure 1), engineered only to express enhanced green fluorescent protein (EGFP). All 6 mice treated with 10^7 pfu of KG and 2 of the 6 treated with 10^4 pfu of KG exhibited signs of infection outside of the tumors, such as skin erosions or leg fasciculations, within 12 days after injection and died before tumor volumes reached the equivalent of 10% of body weight. In contrast, none of the mice treated with KGNE or KGΔ showed such signs during the observation period. These results encouraged us to test the characteristics of the anti-tumor effects of these oHSVs when the syncytial mutations are introduced.

The hEGFR-specific RR-oHSV with syncytial mutations mediates markedly more robust anti-tumor effects than that without the syncytial mutations

We first compared the *in vitro* characteristics of the syncytial derivatives of KGNE and KGΔ, each of which contains the pair of syncytial mutations gB:R858H and gK:A40T (termed BhKt hereafter). As shown in Figure 3A, whereas KGΔ-BhKt (Figure 1) and KGNE-BhKt[24] each developed syncytia of similar morphology, KGΔ and KGNE did not form syncytia but caused rounding of the infected cells, as is typical of wild-type HSV-1 infection. Although the introduction of the syncytial mutations caused significant enlargement of plaques formed by both KGΔ and KGNE (each p < 0.05), the resultant areas of plaques formed by KGΔ-BhKt and KGNE-BhKt were similar (p = 0.69) (Figure 3B). Likewise, although the introduction of the syncytial mutations caused significant enhancement of cell killing activities by both KGΔ and KGNE (each p < 0.05), the cell killing activities of KGΔ-BhKt and KGNE-BhKt were similar (multiplicity of infection [MOI] 0.001, p = 0.96; MOI 0.01, p = 0.94; MOI 0.1, p = 0.91) (Figure 3C). These results suggest that the two viruses, KGNE-BhKt and KGΔ-BhKt, induce syncytia of similar size and morphology in monolayer cultures of U87 cells and kill these cells with similar efficiencies *in vitro*.

We also examined whether *in vivo* treatment using either KGNE-BhKt or KGΔ-BhKt caused syncytium formation in U87 xenografts in a qualitative manner. Consecutive tumor sections were prepared 3 days after intra-tumoral injection and stained with hematoxylin and eosin or immunostained for EGFP expression. In the tumors injected with KGΔ or KGNE, extensive ballooning degeneration was observed, with some of the degenerated cells containing ground-glass nuclei (Figure 4). The intensities of cytosolic EGFP staining were quite different among the individual infected cells, suggesting that cell-cell fusion was not induced by KGΔ or KGNE *in vivo*. These features were considered to be typical of wild-type HSV-1 infection. In contrast, in the tumors injected with KGΔ-BhKt or KGNE-BhKt, multinucleated giant cells were observed frequently (Figure 4). Infection with KGΔ-BhKt or KGNE-BhKt, unlike KGΔ or KGNE, caused formation of large areas of homogeneous cytosolic EGFP staining that each contained multiple nuclei. These results demonstrate that syncytial mutations introduced into the genome of KGΔ or KGNE cause syncytium formation in U87 xenografts *in vivo*.

Next, we examined the impact of introducing syncytial mutations on the *in vivo* anti-tumor effects of KGNE. We treated subcutaneous U87 tumors (~300 mm^3) with a single intra-tumoral injection of PBS, KGNE (10^2 or 10^3 pfu), or KGNE-BhKt (10^1, 10^2, or 10^3 pfu). Tumor growth was significantly suppressed by treatment with 10^3 pfu of KGNE (p < 0.0001) but not with control PBS or 10^2 pfu of KGNE (p = 0.62) (Figure 5A). However, no tumor showed complete regression with this treatment. In contrast, tumor growth was significantly suppressed by treatment using either 10^1, 10^2, or 10^3 pfu of KGNE-BhKt even compared to 10^3 pfu of KGNE (p < 0.0001 for each dose), and all the tumors regressed during the observation period (Figure 5A).

We also treated larger tumors of ~780 mm^3 23 days after inoculation with a single intra-tumoral injection of 10^7 pfu of KGNE, 10^2 pfu of KGNE-BhKt, or PBS as a control. Injection of 10^7 pfu of KGNE had no significant effects on tumor growth, and all the mice had to be euthanized within 15 days after starting this treatment (Figures 5B and 5C). In contrast, the tumors in 5 of 6 mice treated with 10^2 pfu of KGNE-BhKt showed significant growth suppression by 5–10 days and disappeared within 35 days after starting treatment (Figure 5B). Mice treated with 10^2 pfu of KGNE-BhKt had significantly better overall survival than those treated with 10^7 pfu of KGNE (p < 0.01) (Figure 5C). These results might suggest that the magnitude of the anti-tumor effect of KGNE-BhKt is at least 100,000-fold greater than that of the original KGNE.
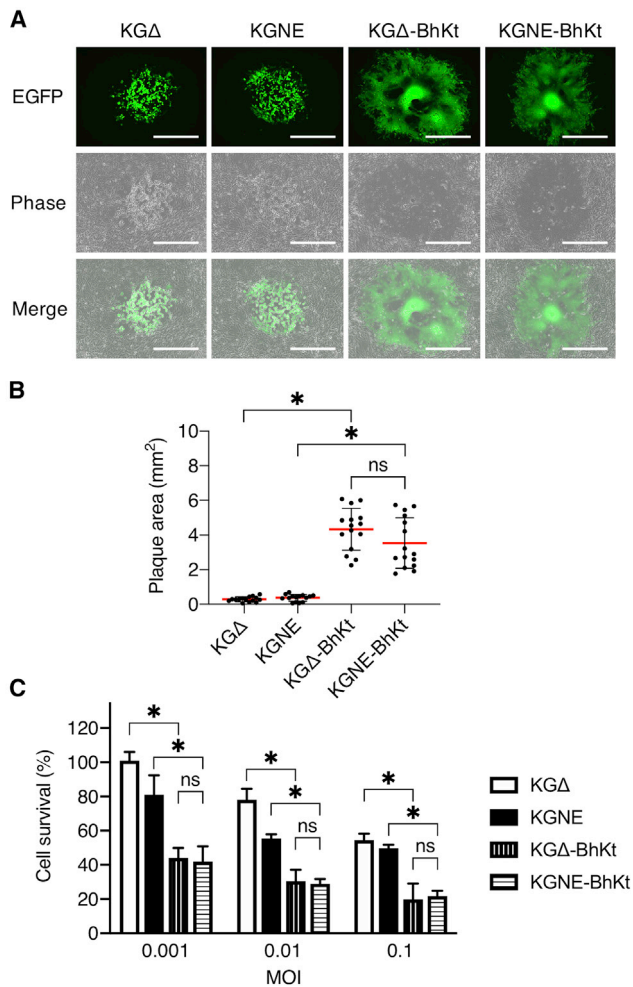
A

EGFP

KGΔ   KGNE   KGΔ-BhKt   KGNE-BhKt

Phase

Merge

B

C

Figure 3. *In vitro* plaque formation and cell killing by the syncytial derivatives of hEGFR-specific RR-oHSV and ICP34.5-deleted CR-oHSV

(A) U87 cells were infected with the viruses shown above the panels and overlaid with methylcellulose-containing medium. EGFP signals and phase-contrast images were recorded 2 days post-infection. Photographs of representative plaques are shown. Scale bars, 500 μm. (B) U87 cells were infected with the viruses shown below the graph and overlaid with methylcellulose-containing medium. Areas of plaques 3 days post-infection are shown (n = 15). Means ± standard deviations (SDs) are also shown. Dunn's test was used for comparative analysis. *p < 0.05; ns, not significant. (C) U87 cells were infected at MOIs indicated below the graph for 3 days, and cell viability relative to uninfected cells was assessed by MTT assay. Means ± SDs are shown (n = 6). Sidak test was used for comparative analysis. *p < 0.05; ns, not significant. White bars, KGΔ; black bars, KGNE; vertical-striped bars, KGΔ-BhKt; horizontal-striped bars, KGNE-BhKt. Experiments were repeated twice, and similar results were observed.

The ICP34.5-deleted CR-oHSV with syncytial mutations mediates anti-tumor effects superior to the original CR-oHSV but only to a modest degree

Next, we examined the anti-tumor effects of the KGΔ with BhKt mutations. The U87 tumor xenografts (∼320 mm^3) were treated with a single intra-tumoral injection of KGΔ at 10^7 pfu, KGΔ-BhKt

at 10^1, 10^3, 10^5, or 10^7 pfu, or PBS as a control. KGNE-BhKt at 10 pfu was also used for comparison. The growth of tumors in the animals treated with 10^3, 10^5, or 10^7 pfu of KGΔ-BhKt was significantly suppressed compared to those treated with PBS (10^3, p < 0.01; 10^5 and 10^7, p < 0.0001), but 10^1 pfu of KGΔ-BhKt caused no significant tumor growth suppression (p = 0.72) (Figure 5D). Compared with the treatment with 10^7 pfu of KGΔ, the magnitude of tumor suppression was significantly superior with 10^5 pfu or 10^7 pfu of KGΔ-BhKt (10^5, p < 0.01; 10^7, p < 0.0001) (Figure 5D). Compared with the effect of 10^7 pfu of KGΔ-BhKt, tumor growth in the mice treated with only 10 pfu of KGNE-BhKt was significantly more suppressed (p < 0.0001) and resulted in complete regression in all 6 mice tested (Figure 5D). These results suggest that one of our RRsyn-oHSVs, KGNE-BhKt, has a potent anti-tumor effect up to 1,000,000-fold greater than KGΔ-BhKt, a syncytial derivative of CR-oHSV, in this model.

A single intra-venous administration of RRsyn-oHSVs results in potent anti-tumor effects

Based on the observation that intra-tumoral injection of as few as 10 pfu of KGNE-BhKt resulted in complete regression of U87 xenografts, we hypothesized that systemic administration of KGNE-BhKt might yield significant anti-tumor effects. To test this hypothesis, U87 subcutaneous tumor xenografts at relatively large sizes (∼700 mm^3, 21 days after tumor inoculation) were treated with a single injection of 10^5 or 10^7 pfu of KGNE-BhKt via the tail vein. Whereas the tumors in PBS-treated mice grew to >2,000 mm^3 within as little as 7 days, tumors in all of the mice treated with intra-venous injection of KGNE-BhKt regressed and disappeared within 35 days (Figure 6A). During the observation period, none of the mice treated with systemic KGNE-BhKt suffered regrowth of the tumor, any signs of off-tumor virus infection such as skin erosions or leg fasciculations, or apparent abnormalities reminiscent of severe systemic inflammation. The tumor samples were harvested 1 or 3 days after tail vein injection of 10^7 pfu of KGNE-BhKt and immune-stained for EGFP to evaluate virus spread *in vivo*. We found multiple EGFP-positive syncytia each containing 30–200 nuclei in the samples harvested 1 day after the injection (Figure 6B; Figure S1). In the samples harvested 3 days after the injection, very large, coalesced EGFP-stained areas were observed in the tumor (Figure 6B). These observations suggest that the highly robust anti-tumor effects of KGNE-BhKt that were observed in Figures 5A and 5B and Figure 6A were caused by the vigorous, progressive spread of KGNE-BhKt within the tumor.

We also examined tumor models other than U87 to exclude the possibility that the robustness of our RRsyn-oHSVs could be limited to U87 xenografts. The growth of HepG2 tumor xenografts, which express both EGFR and EpCAM,[22] was also significantly suppressed after intra-venous injection of either KGNE-BhKt or KGNEp-BhKt (Figure 1),[24] an hEpCAM-specific RRsyn-oHSV (p < 0.0001 compared to PBS for each virus) (Figure 6C). In contrast, injection of KGNEp-BhKt did not affect the growth of U87 xenografts, which express EGFR but no EpCAM[22] (p = 0.90 compared to PBS) (Figure 6D). These results clearly show that the anti-tumor effects of
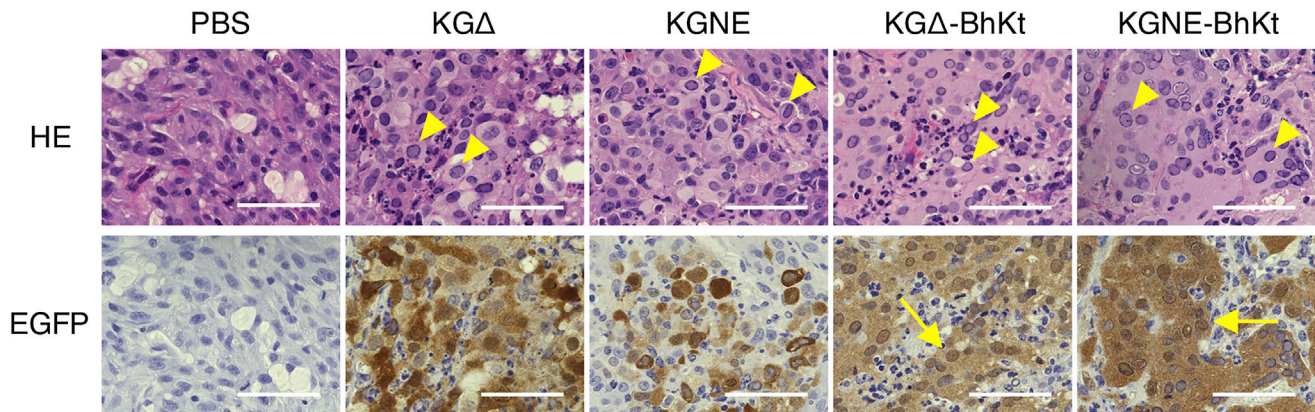
Figure 4. Syncytium formation in U87 xenografts caused by the syncytial derivatives of hEGFR-specific RR-oHSV and ICP34.5-deleted CR-oHSV

U87 cells were injected subcutaneously into SCID-beige mice, and, when tumor volumes reached >780 mm³, PBS or 10⁵ pfu of KGΔ, KGNE, KGΔ-BhKt, or KGNE-BhKt was injected into the tumors. Consecutive tumor sections were prepared 3 days post-injection and stained with hematoxylin and eosin (HE; upper) or immunostained for EGFP expression (lower). Arrowheads, ground-glass nuclei; Arrows, multinucleated giant cells. Scale bars, 50 μm.

the RR-oHSVs with BhKt mutations are strictly limited to tumors expressing the targeted receptors.

Syncytia induced by RRsyn-oHSVs consist exclusively of cancer cells and survive for longer periods of time than those induced by the syncytial CR-oHSV, which consist of both cancer and non-cancerous cells

As shown above, *in vivo* treatment with KGNE-BhKt yielded significantly more robust anti-tumor effects than treatment with KGΔ-BhKt. To explore the mechanisms responsible for this difference, we used an *in vitro* two-cell-culture model consisting of not only cancer cells but also non-cancerous cells to better mimic *in vivo* conditions. U87 cells were infected with KGΔ-BhKt or KGNE-BhKt at low MOIs in advance, seeded together with U87 cells expressing mCherry (U87-mCherry) or non-cancerous 3T6 cells expressing mCherry (3T6-mCherry), overlaid with methylcellulose-containing medium, and observed for syncytium formation by time-lapse microscopy. The 3T6 murine fibroblasts were employed because they have been frequently used as non-cancerous normal cells in the assessment of CR-oHSVs elsewhere.[31–33] When U87 cells infected with KGΔ-BhKt or KGNE-BhKt were seeded together with U87-mCherry cells, syncytia generated by either virus continued to expand to similar degrees (Figure 7A; Video S1). Thus, these two viruses have similar capabilities for syncytium formation in cultures containing only U87 tumor cells. However, the appearance and behavior of the syncytia was quite different when 3T6-mCherry cells were seeded together. When KGΔ-BhKt-infected U87 cells were used, the syncytia showed both EGFP and mCherry signals, suggesting that they included both U87 and 3T6 cells. They expanded for some time (∼39 hours post-infection [hpi]), but both fluorescent signals suddenly disappeared at the same time (Figure 7A; Video S2). In contrast, when KGNE-BhKt-infected U87 cells were used, the resultant syncytia showed no mCherry signals, suggesting that they were composed

exclusively of U87 cells and did not include 3T6-mCherry cells because of the strict receptor specificity at initial cell entry and on subsequent cell-cell spread of our RRsyn-oHSVs as shown in our previous report.[24] These syncytia continuously grew larger throughout the observation period of 29–48 hpi (Figure 7A; Video S2).

To assess the fate of the cells, U87 cells infected with either virus were seeded together with uninfected 3T6 or U87 cells in the presence of SYTOX Orange to detect cell death, and the sizes of the syncytia were monitored until cell death or up to 78 hpi. In the cultures consisting of U87 and 3T6 cells, syncytia generated by KGNE-BhKt remained unstained with SYTOX and continued to expand, reaching ∼5 mm² at the end of the observation period (Figure 7B). In contrast, cell death occurred in all of the KGΔ-BhKt syncytia by 48 hpi, which reached only ∼0.5 mm² before cell death (Figure 7B). In the cultures of only U87 cells, the degree of syncytium expansion caused by either virus was not significantly different (78 hpi, p = 0.10) (Figure 7B). These results might indicate that incorporation of 3T6 fibroblasts, which only happens in KGΔ-BhKt syncytia, results in relatively early termination of expansion because of the cell death.

To further assess the responsible mechanisms, KGΔ-BhKt- or KGNE-BhKt-infected U87 cells were seeded together with hEGFR-transduced 3T6 cells (3T6-hEGFR) or mock-transduced 3T6 cells. As shown in Figure 7C, when KGΔ-BhKt infected U87 cells were seeded together with either 3T6-hEGFR or mock-transduced 3T6 cells, but not with U87 cells, the syncytia became SYTOX positive and at least partially lost EGFP signals, indicative of cell death in the syncytia, 5 days post-infection. In contrast, when KGNE-BhKt-infected U87 cells were seeded together with mock-transduced 3T6 cells, the resultant syncytia remained unstained with SYTOX and continued to expand (Figure 7C), in agreement with the observations in Figures 7A and 7B. Importantly, however, when KGNE-BhKt-infected U87

A

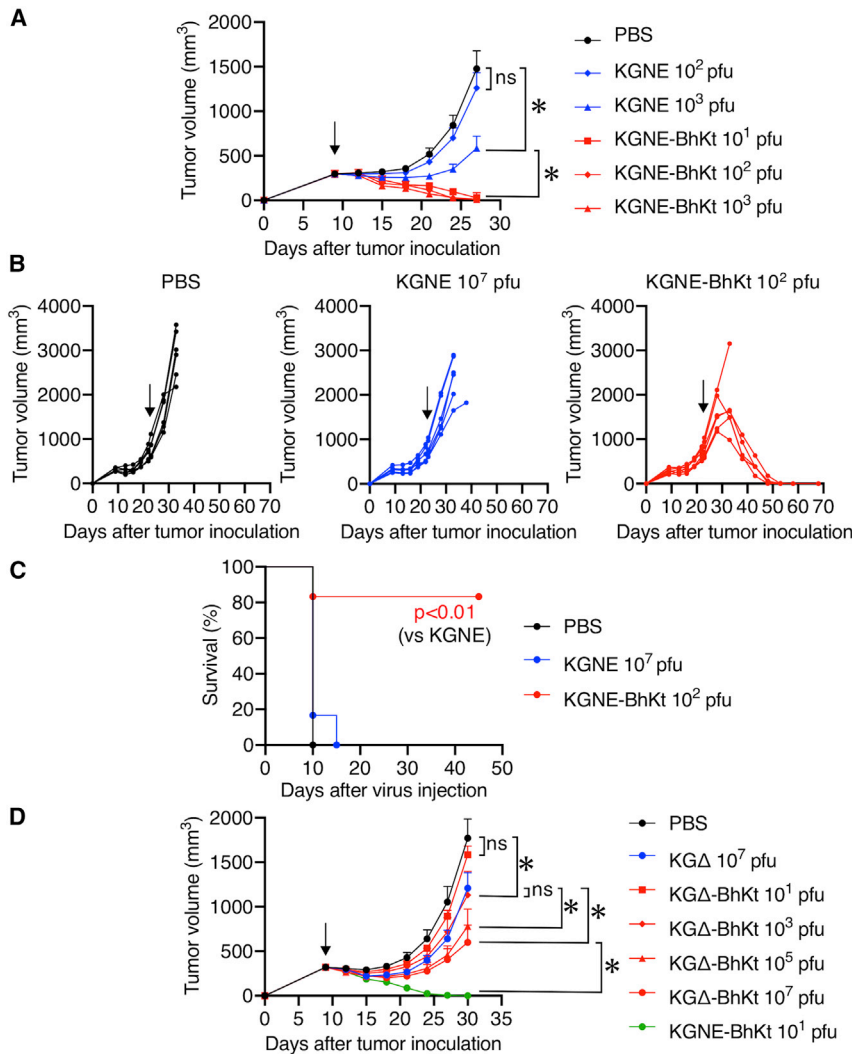**B** PBS | KGNE 10^7 pfu | KGNE-BhKt 10^2 pfu

C

D

Figure 5. Effects of the introduction of syncytial mutations into hEGFR-specific RR-oHSV and ICP34.5-deleted CR-oHSV on the efficiency of anti-tumor activity when injected intra-tumorally

(A) U87 cells were injected subcutaneously into SCID-beige mice, and, when tumor volumes reached ~300 mm^3 (arrow), PBS (black circles; n = 6), 10^2 (blue diamonds; n = 6) or 10^3 (blue triangles; n = 6) pfu of KGNE, or 10^1 (red squares; n = 6), 10^2 (red diamonds; n = 6), or 10^3 (red triangles; n = 6) pfu of KGNE-BhKt was injected into the tumors. Tumor volumes were measured, and mean volumes ± SEs are shown. Two-way repeated-measures ANOVA was used for comparative analysis. *p < 0.05; ns, not significant. (B) PBS (left; n = 6), 10^7 pfu of KGNE (center; n = 6), or 10^2 pfu of KGNE-BhKt (right; n = 6) were intra-tumorally injected into SCID-beige mice bearing subcutaneous U87 xenografts (~780 mm^3, 23 days after inoculation; arrows). Tumor volumes were measured and plotted. (C) Survival of the mice in (B) was monitored and is shown in a Kaplan-Meier plot. Log-rank testing was used for comparative analysis. Black line, PBS; blue line, 10^7 pfu of KGNE; red line, 10^2 pfu of KGNE-BhKt. (D) PBS (black circles; n = 6), 10^7 pfu of KGΔ (blue circles; n = 6), 10^1 (red squares; n = 6), 10^3 (red diamonds; n = 6), 10^5 (red triangles; n = 6), or 10^7 (red circles; n = 6) pfu of KGΔ-BhKt, or 10^1 pfu of KGNE-BhKt (green circles; n = 6) was intra-tumorally injected into SCID-beige mice bearing subcutaneous U87 xenografts (~320 mm^3; arrow). Tumor volumes were measured, and mean volumes ± SEs are shown. Two-way repeated-measures ANOVA was used for comparative analysis. *p < 0.05; ns, not significant. Experiments were repeated twice, and similar results were observed.

cells were seeded together with 3T6-hEGFR cells, the resultant syncytia became positive for SYTOX at this point (Figure 7C). These results strongly suggest that the observed cell death in syncytia was triggered as a result of the involvement of non-cancerous cells (i.e., formation of hybrid syncytia composed of both cancer and non-cancerous cells) and does not require the ICP34.5 deletions in the virus.

Similar results were obtained in the same assay using KGNEp-BhKt, which can bind to human but not to murine EpCAM, and the different cell combinations consisting of HepG2 and 3T6 cells or HepG2 and MS1 cells (a murine vascular endothelial line) (Figure 7D). To mitigate the concern that this phenomenon was caused by the artificial condition involving cell lines from different species, human and mouse, we performed the same assay using 3T6 and murine hepatoma Hepa1-6 cells transduced with hEpCAM, instead of HepG2. As shown in Figure 7E, similar results were also observed in this assay. Furthermore, we also performed the same assay using

human pulmonary microvascular endothelial cells (HPMECs) instead of 3T6 cells, along with HepG2 cells, and obtained similar results (Figure 7F). Thus, it would be justified to assume that the cell death of syncytia caused by CRsyn-oHSV might be induced earlier than that by RRsyn-oHSV as a result of the involvement of cell death-inducing non-cancerous cells.

These results strongly suggest that the RRsyn-oHSVs exert robust anti-tumor effects *in vivo* because they can cause the formation of tumor-only syncytia, which would expand for prolonged periods.

DISCUSSION

We have shown in this study that the introduction of syncytial mutations significantly enhances the *in vivo* anti-tumor effects of either RR-oHSV or an ICP34.5-deleted CR-oHSV. We have also shown that the magnitude of the anti-tumor effects is remarkably more robust in RR-oHSV with syncytial mutations (RRsyn-oHSV) than in CR-oHSV with syncytial mutations (CRsyn-oHSV). After only a single intra-tumoral injection of RRsyn-oHSV at an extremely low dose, all treated tumors regressed completely. Furthermore, the intra-venous administration of RRsyn-oHSV mediated significant
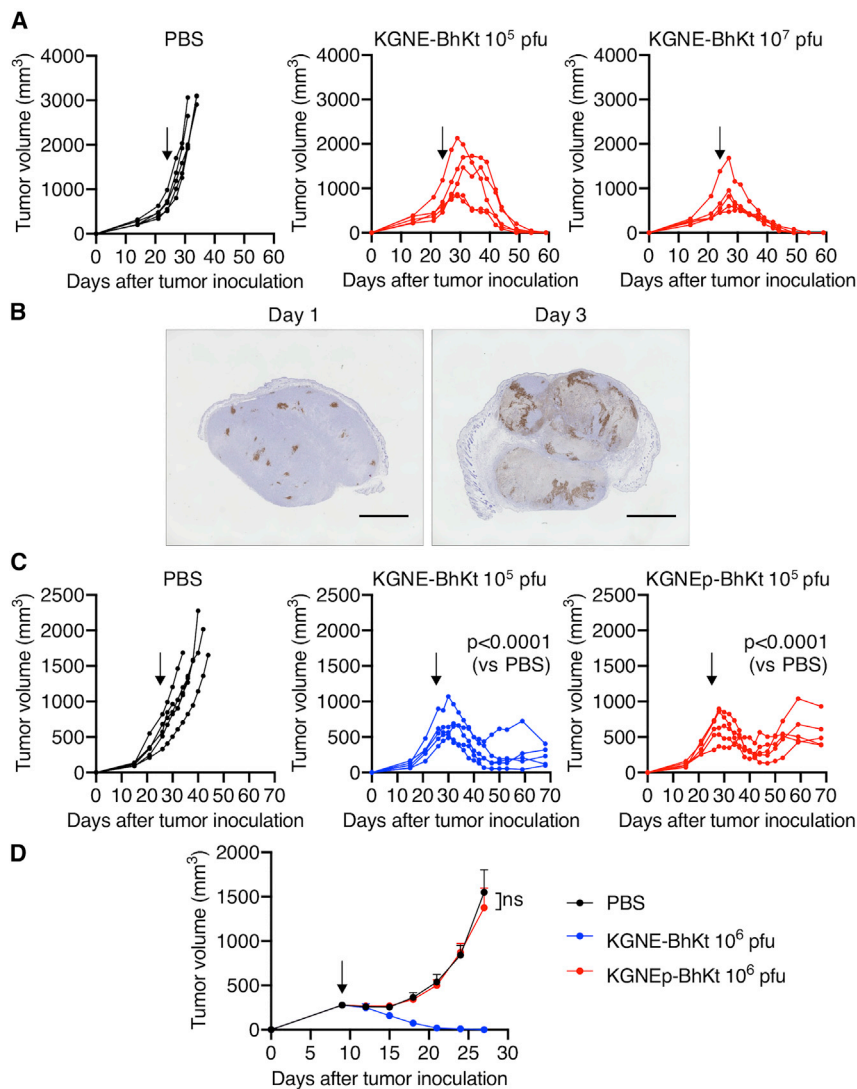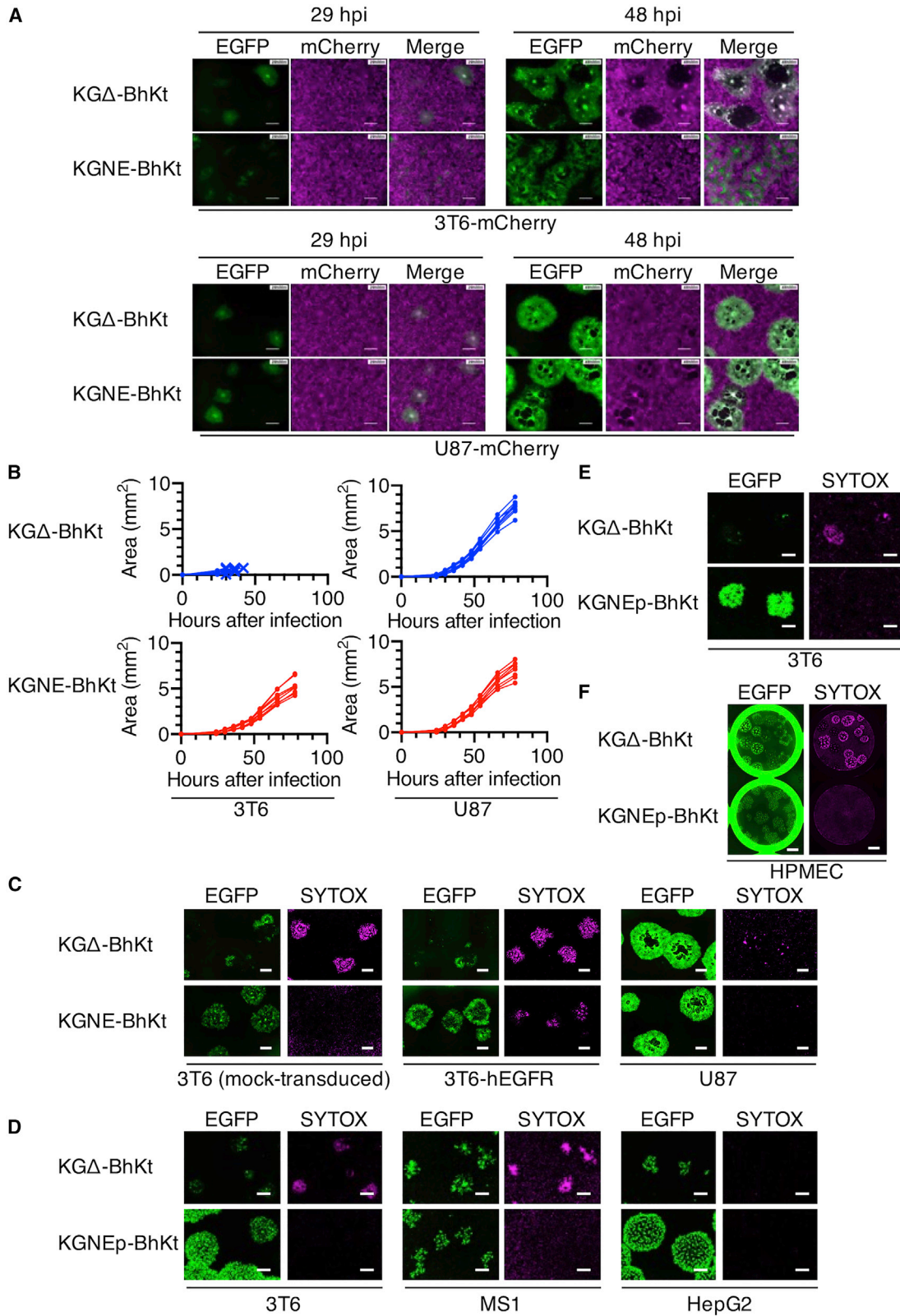
Figure 6. Efficiency of anti-tumor activity of a single intra-venous injection of the syncytial derivatives of the hEGFR- or hEpCAM-specific RR-oHSVs

(A) PBS (left; n = 5) or 10^5 (center; n = 5) or 10^7 (right; n = 5) pfu of KGNE-BhKt was injected into SCID-beige mice bearing subcutaneous U87 xenografts (~700 mm³, 24 days after inoculation; arrows) via the tail vein. Tumor volumes were measured and plotted. (B) KGNE-BhKt (10^7 pfu) was injected into SCID-beige mice bearing subcutaneous U87 xenografts (~400 mm³) via the tail vein. Tumor sections were prepared 1 or 3 days post-injection and immunostained for EGFP expression. Scale bars, 2 mm. See also Figure S1. (C) PBS (left; n = 5) or 10^5 pfu of KGNE-BhKt (center; n = 5) or KGNEp-BhKt (right; n = 5) was injected into SCID-beige mice bearing subcutaneous HepG2 xenografts (~580 mm³, 26 days after inoculation; arrows) via the tail vein. Tumor volumes were measured and plotted. Two-way repeated-measures ANOVA was used for comparative analysis. (D) PBS (black circles; n = 6) or 10^6 pfu of KGNE-BhKt (blue circles; n = 6) or KGNEp-BhKt (red circles; n = 6) was injected into SCID-beige mice bearing subcutaneous U87 xenografts (~280 mm³, 9 days after inoculation; arrow) via the tail vein. Tumor volumes were measured and mean volumes ± SEs are shown. Two-way repeated-measures ANOVA was used for comparative analysis. ns, not significant. Experiments were repeated twice, and similar results were observed.

anti-tumor effects even against large tumors. If CR-oHSVs are administered intravenously, it is inferred that a significant fraction thereof would initially enter non-cancerous cells, which do not allow virus replication, and are therefore lost before encountering cancer cells. This situation could be avoided by our RR-oHSVs because they are engineered not to enter cells through the natural HSV receptors expressed on a wide variety of cells including non-cancerous cells. Thus, our RR-oHSVs appear to be far more suitable for systemic administration than CR-oHSVs, which might be a beneficial property for treating the multiple distant metastases often found in advanced cancer patients.

The *in vivo* treatment models we employed in the current study were human tumor xenografts in immunodeficient mice. Since the xenograft tumor model is suitable for the assessment of the direct oncolytic potency of the viruses, it has been commonly used by multiple investigators of oHSVs even for preclinical evaluation.[34] However, it should be noted that our RRsyn-oHSVs, which bind human but not murine antigens, have optimal cancer specificity in this model. Since such optimal cancer specificity can hardly be expected for most membrane-bound tumor-associated antigens in the clinical setting, careful selection of highly cancer-specific antigen-antibody pairs would be required to replicate our experimental results (i.e., robust efficacy and safety) in humans. It should also be noted that our results do not reflect any adaptive immunological responses against either oHSVs or tumor cells. If RRsyn-oHSVs are tested in immune-competent animals, immunological responses against the RRsyn-oHSVs would be induced, which could lead to a decreased number of infectious virus particles available for tumor cell infection and/or attenuated syncytium formation or expansion, thus reducing the anti-tumor effects of the RRsyn-oHSVs. On the other hand, immunological responses against tumor cells might also be induced and could increase the anti-tumor effects of the RRsyn-oHSVs. Multiple investigators using oHSVs and other oncolytic viruses have shown that potent anti-tumor immune responses can be induced by tumor cells that have been lysed by oncolytic viruses via a mechanism similar to vaccination.[35,36] In addition, it has been reported that cell death of syncytia tends to show multiple features of immunogenic cell death.[37] It is of great interest to examine the magnitude and the specificity of anti-tumor

A

29 hpi / 48 hpi — EGFP, mCherry, Merge

KGΔ-BhKt, KGNE-BhKt

3T6-mCherry

29 hpi / 48 hpi — EGFP, mCherry, Merge

KGΔ-BhKt, KGNE-BhKt

U87-mCherry

B

KGΔ-BhKt, KGNE-BhKt

Area (mm²) vs Hours after infection

3T6, U87

C

EGFP, SYTOX

KGΔ-BhKt, KGNE-BhKt

3T6 (mock-transduced), 3T6-hEGFR, U87

D

EGFP, SYTOX

KGΔ-BhKt, KGNEp-BhKt

3T6, MS1, HepG2

E

EGFP, SYTOX

KGΔ-BhKt, KGNEp-BhKt

3T6

F

EGFP, SYTOX

KGΔ-BhKt, KGNEp-BhKt

HPMEC

(legend on next page)

immunity following the robust direct oncolysis achieved by our RRsyn-oHSV. Thus, further examination using syngeneic mouse tumors in immune-competent mice might be helpful in predicting anti-tumor effects in cancer patients.

We examined the mechanisms responsible for the distinctively potent anti-tumor effects of RRsyn-oHSV compared with CRsyn-oHSV using two-cell-culture system assays. In such assays, we showed that infection with CRsyn-oHSV allowed the syncytia to include non-cancerous cells, which appeared to induce the cell death of syncytia. However, such a phenomenon was not observed with RRsyn-oHSV. Further work is necessary to elucidate the exact molecular signals responsible for this death induction of syncytia.

In addition, another possible mechanism might be associated with a different susceptibility to type I interferons (IFNs) between cancer cells and non-cancerous cells. Different from non-cancerous cells, many cancer cells exhibit unresponsiveness to type I IFNs, allowing oncolytic viruses to replicate efficiently.[8] However, CRsyn-oHSV would allow the syncytia to include non-cancerous cells, which might force the syncytia to restore responsiveness to type I IFNs. In contrast, the syncytia formed with RRsyn-oHSV would not include non-cancerous cells and thus would remain resistant to type I IFNs.

Other investigators have reported favorable anti-tumor effects using different CR-oHSVs with hyperfusogenic capability.[38–41] Whereas we utilized syncytial mutations that had been identified in naturally occurring HSV-1 isolates as a means of conferring hyperfusogenicity on oHSVs, others have used a different approach in which CR-oHSVs were engineered to express gibbon ape leukemia virus envelope fusogenic membrane glycoprotein (GALV-FMG) as a foreign transgene.[38–41] Nakamori and colleagues reported the construction of the Synco-2 strain by inserting an expression cassette for GALV-FMG into the genome of an ICP34.5-deleted CR-oHSV and showed enhanced anti-tumor effects in their tumor model.[39] Similarly, Thomas and colleagues inserted a GALV-FMG expression cassette into a CR-oHSV that contains the same genetic modifications as T-VEC.[41] Since human Pit-1 but not murine Pit-1 functions as the receptor for GALV-FMG,[42–45] the syncytia generated by these GALV-FMG-expressing CR-oHSVs would not involve any non-cancerous mouse cells in mouse models. Therefore, their mouse model would not have been affected by the premature termination of syncytium expansion that we found in the current study. This im-

plies that the favorable results in mouse models reported by these investigators might not be similar in humans. In contrast, RRsyn-oHSVs retargeted to tumor-associated antigens that are scarcely expressed on the non-cancerous cells within the tumor would avoid the inclusion of non-cancerous cells into the syncytia in human tumors.

Taken together, the results of the present study suggest that our RRsyn-oHSVs equipped with scFvs specific for appropriately selected targets could be useful tools for developing novel effective treatments against various types of cancer, especially those with multiple metastatic lesions not easily accessible for direct intra-tumoral injection.

MATERIALS AND METHODS
Cells

Human glioblastoma U87 (ATCC HTB-14), human hepatoblastoma HepG2 (ATCC HB-8065), African green monkey kidney Vero (ATCC CCL-81), and hEpCAM-transduced Vero-EpCAM cells were cultured as described previously.[22] Murine fibroblast 3T6 (ECACC 86120801) and murine hepatoma Hepa1-6 (ATCC CRL-1830) cells were cultured in Dulbecco's modified Eagle's medium (DMEM; Thermo Fisher Scientific, Waltham, MA, USA) supplemented with 10% fetal bovine serum (FBS; Thermo Fisher Scientific). Murine vascular endothelial MS1 cells (ATCC CRL-2279) were cultured in DMEM supplemented with 5% FBS. HPMECs (PromoCell, Heidelberg, Germany) were cultured in KBM VEC-1 (Kojin Bio, Saitama, Japan). U87-mCherry and 3T6-mCherry cells were established by transfection of U87 or 3T6 cells with an expression plasmid for mCherry under control of the HCMV-IE promoter and selected for resistance to 2 or 4 μg/mL puromycin (Thermo Fisher Scientific), respectively. 3T6-hEGFR cells were established by infection of 3T6 cells with an hEGFR-expressing retroviral vector derived from pMXc-puro (provided by Toshio Kitamura, University of Tokyo, Tokyo, Japan) that was produced as described previously[22] and selected for resistance to 4 μg/mL puromycin. Similarly, Hepa1-6-hEpCAM cells were established by infection of Hepa1-6 cells with a hEpCAM-expressing retroviral vector and selected for resistance to 2 μg/mL puromycin.

HSV-BAC recombineering

All HSV-bacterial artificial chromosome (BAC) constructs generated in this study were derived from KOS-37 BAC[46] (provided by David Leib, Dartmouth Medical School, Hanover, NH, USA). All BAC recombinations were performed with scarless gene modification

Figure 7. In vitro expansion of syncytia generated by the syncytial derivatives of the ICP34.5-deleted CR-oHSV and hEGFR- or hEpCAM-specific RR-oHSVs
(A) U87 cells were infected with viruses shown on the left at an MOI of 0.00015 for 2 h, seeded in combination with the same number of cells indicated below the panels, and overlaid with methylcellulose-containing media. Mixed cultures were observed for EGFP and mCherry signals in a time-lapse manner. Photographs at 29 or 48 hpi are shown (see time-lapse movies in Videos S1 and S2). (B) U87 cells were infected with viruses shown on the left at an MOI of 0.000004 for 2 h, seeded in combination with the same number of cells indicated below the graphs, and overlaid with media containing methylcellulose and SYTOX Orange. Eight syncytia were monitored during the period of 24–78 hpi. Areas of syncytia were measured and plotted. Two-tailed Mann-Whitney U test was used for comparative analysis. ×, last measurement before becoming positive for SYTOX Orange staining. (C–F) U87 (C), HepG2 (D and F), or Hepa1-6-hEpCAM (E) cells were infected with viruses shown on the left at MOIs of 0.000006–0.0003 for 2 h, seeded in combination with the same (C–E) or double (F) number of cells indicated below the panels, and overlaid with media containing methylcellulose and SYTOX Orange. Mixed cultures were observed for EGFP and SYTOX signals 5 (C), 4 (D and F), or 2 (E) days post-infection, respectively. Experiments were repeated twice, and similar results were observed. Scale bars, 500 μm (A, D, and E), 1 mm (C), or 2 mm (F).

based on the Red recombination system and the plasmids pRed/ET (Gene Bridges, Heidelberg, Germany) and pBAD-I-SceI (provided by Nikolaus Osterrieder, Free University of Berlin, Berlin, Germany). All constructs were confirmed by PCR analysis, pulsed-field gel electrophoresis analysis of restriction enzyme digests, and targeted DNA sequencing. Transfer constructs for Red recombination were generated as described previously.[47] Briefly, the kanamycin-resistance gene flanked by an I-SceI restriction site (I-SceI-aphAI fragment) was amplified from pEPkan-S2 (also provided by Nikolaus Osterrieder) by PCR with the different targeting primers as specified below. All targeting fragments for Red recombination were purified with a FastGene Gel/PCR Extraction Kit (NIPPON Genetics, Tokyo, Japan) or a QIAGEN gel extraction kit (QIAGEN, Hilden, Germany). The BAC construct pKG was generated by the insertion of an EGFP expression cassette between the U_L3 and U_L4 genes of KOS-37 BAC by the same method as used in the previous study.[22] The BAC construct pKGΔ was generated by deleting the region containing codon 46 to the stop codon of both of the two ICP34.5 open reading frames in a step-by-step manner. The transfer construct containing ICP34.5-codon45-I-SceI-aphAI-ICP34.5-codon45-3′ UTR was obtained by PCR using pEPkan-S2 as the template, with the primers 5′-CCCAGGTAACCTCCACGCCCAACTCGGAACCCGTGGTCA GGAGCGCGCCCAGGATGACGACGATAAGTAGGG-3′ and 5′-GACGACTCGGCGGACGCTGGTTGGCCGGGCCCCGCCGCGC TGGCGGCCGCGGGCGCGCTCCTGACCACGGGTTCCGAGTTG GGCGTGGAGGTTACCTGGGCTACAACCAATTAACCAATTCT GATTAG-3′, and was used for recombination with the ICP34.5 region in TRL of pKG, followed by aphAI gene removal, resulting in pKGΔ-t. The same transfer construct was then used for recombination with the ICP34.5 region in IRL of pKGΔ-t, followed by aphAI gene removal, resulting in pKGΔ. The BAC construct pKGΔ-BhKt was generated by exchanging the codon for arginine (CGC) at residue 858 in the gB with a codon for histidine (CAT) and the codon for alanine (GCG) at residue 40 in the gK with a codon for threonine (ACC), respectively, of pKGΔ in a step-by-step manner, as described previously.[24]

Viruses

Recombinant viruses KGNE, KGNE-BhKt, KGNEp, and KGNEp-BhKt have been described previously.[22,24] KG, KGΔ, and KGΔ-BhKt were established by cotransfection of Vero or Vero-EpCAM cells with pKG, pKGΔ, or pKGΔ-BhKt, respectively, and pxCANCre (provided by Izumu Saito, University of Tokyo, Tokyo, Japan), followed by two rounds of limiting dilution on Vero or Vero-EpCAM cells. Confirmation of BAC deletion was carried out as described previously.[48] Viruses were titered on Vero or Vero-EpCAM cells that express hEpCAM ectopically and simian EGFR as described previously[49]; Vero EGFR is recognized by the anti-EGFR scFv used in this study. The propagation and purification of the viruses were essentially as described previously.[50]

Plaque formation and cell killing assays

Plaque formation and cell killing assays were performed essentially as described previously[21,22] with a BZ X-700 or -800 fluorescence micro-

scope (Keyence, Osaka, Japan) and a Synergy Neo2 microplate reader (BioTek, Winooski, VT, USA), respectively.

Assessments of syncytium expansion in the presence of both cancer and non-cancerous cells

Singly suspended cancer cells were incubated with viruses at low MOIs at 37°C for 2 h with rotation, co-seeded with an equal or double number of uninfected non-cancerous cells, and overlaid with media containing 1% methylcellulose (Wako, Osaka, Japan) and, in some experiments, with 0.5 μM SYTOX Orange (Thermo Fisher Scientific). Plaques were observed under the BZ X-700 or -800 microscope.

Animal experiments

All animal experiments were approved by the Animal Care and Use Committee at The Institute of Medical Science, The University of Tokyo, and conducted according to institutional guidelines. Six- to eight-week-old female SCID-beige mice (CB17.Cg-$Prkdc^{scid}Lyst^{bg-J}$/CrlCrlj; Charles River Laboratories Japan, Kanagawa, Japan) were injected subcutaneously with 10^7 human tumor cells suspended in Hank's balanced salt solution (Thermo Fisher Scientific). When the tumors grew to the appropriate size for each experiment, the mice received single intra-tumoral injections consisting of viruses suspended in 30 μL of PBS or single intra-venous injections consisting of viruses suspended in 200 μL of PBS into the tail vein. Tumor volumes were calculated as (length × width2)/2. Mice were euthanized at a humane endpoint, i.e., when the tumor volume reached the equivalent of 10% of body weight.

Histopathology and immunohistochemistry

Paraffin sections were cut at thicknesses of 3–4 μm on a CTM-180 microtome (Sakura Finetek Japan, Tokyo, Japan), mounted on glass slides, deparaffinized in xylene (Wako), and rehydrated in graded ethanol (Wako). Sections were then stained with hematoxylin (Sakura Finetek Japan) and eosin (Muto Pure Chemicals, Tokyo, Japan). For immunohistochemistry, deparaffinized sections were incubated with 0.3% H_2O_2 (Wako) at room temperature (RT) for 5 min to quench endogenous peroxidase activity. The sections were then incubated with a blocking agent (4% Block Ace; DS Pharma Biomedical, Osaka, Japan) at RT for 10 min, followed by incubation with 1 μg/ml rabbit anti-GFP polyclonal antibody (A-11122; Thermo Fisher Scientific) in 4% Block Ace at 4°C overnight, stained by an EnVision+ kit (Agilent Technologies, Santa Clara, CA, USA) according to the manufacturer's instructions, and counterstained with hematoxylin. Images were obtained by BZ X-700.

Statistical analyses

Comparative analyses of the experimental data were performed with the two-way repeated-measures ANOVA (for comparing changes of tumor volumes), log-rank testing (for comparing survival of mice), two-tailed Mann-Whitney U test or Dunn's test (for comparing size of plaques), or Sidak test (for comparing cell viability). Differences were considered statistically significant at p values < 0.05.

AUTHOR CONTRIBUTIONS
T. Suzuki, H.U., and H.T. contributed to the design of the work. T. Suzuki, T. Shibata, and Y.S. contributed to the acquisition of the data. T. Suzuki, H.U., T. Shibata, Y.S., H.I., M.H.-U., R.H., K.O., S.Y., and H.T. contributed to the analysis and interpretation of the data. T. Suzuki, H.U., and H.T. drafted the work.

DECLARATION OF INTERESTS
H.U. is an inventor of intellectual property licensed to Oncorus, Inc. (Cambridge, MA, USA). R.H. and K.O. are employees of Ono Pharmaceutical Co., Ltd.

REFERENCES

1. Russell, S.J., Peng, K.W., and Bell, J.C. (2012). Oncolytic virotherapy. Nat. Biotechnol. 30, 658–670.

2. Peters, C., and Rabkin, S.D. (2015). Designing Herpes Viruses as Oncolytics. Mol. Ther. Oncolytics 2, 15010.

3. Rampling, R., Cruickshank, G., Papanastassiou, V., Nicoll, J., Hadley, D., Brennan, D., Petty, R., MacLean, A., Harland, J., McKie, E., et al. (2000). Toxicity evaluation of replication-competent herpes simplex virus (ICP 34.5 null mutant 1716) in patients with recurrent malignant glioma. Gene Ther. 7, 859–866.

4. Markert, J.M., Medlock, M.D., Rabkin, S.D., Gillespie, G.Y., Todo, T., Hunter, W.D., Palmer, C.A., Feigenbaum, F., Tornatore, C., Tufaro, F., and Martuza, R.L. (2000). Conditionally replicating herpes simplex virus mutant, G207 for the treatment of malignant glioma: results of a phase I trial. Gene Ther. 7, 867–874.

5. Andtbacka, R.H., Kaufman, H.L., Collichio, F., Amatruda, T., Senzer, N., Chesney, J., Delman, K.A., Spitler, L.E., Puzanov, I., Agarwala, S.S., et al. (2015). Talimogene Laherparepvec Improves Durable Response Rate in Patients With Advanced Melanoma. J. Clin. Oncol. 33, 2780–2788.

6. Chou, J., Kern, E.R., Whitley, R.J., and Roizman, B. (1990). Mapping of herpes simplex virus-1 neurovirulence to gamma 134.5, a gene nonessential for growth in culture. Science 250, 1262–1266.

7. Chou, J., Chen, J.J., Gross, M., and Roizman, B. (1995). Association of a M(r) 90,000 phosphoprotein with protein kinase PKR in cells exhibiting enhanced phosphorylation of translation initiation factor eIF-2 alpha and premature shutoff of protein synthesis after infection with gamma 134.5- mutants of herpes simplex virus 1. Proc. Natl. Acad. Sci. USA 92, 10516–10520.

8. Stojdl, D.F., Lichty, B., Knowles, S., Marius, R., Atkins, H., Sonenberg, N., and Bell, J.C. (2000). Exploiting tumor-specific defects in the interferon pathway with a previously unknown oncolytic virus. Nat. Med. 6, 821–825.

9. Harrington, K.J., Andtbacka, R.H., Collichio, F., Downey, G., Chen, L., Szabo, Z., and Kaufman, H.L. (2016). Efficacy and safety of talimogene laherparepvec versus granulocyte-macrophage colony-stimulating factor in patients with stage IIIB/C and IVM1a melanoma: subanalysis of the Phase III OPTiM trial. OncoTargets Ther. 9, 7081–7093.

10. Andtbacka, R.H.I., Collichio, F., Harrington, K.J., Middleton, M.R., Downey, G., Öhrling, K., and Kaufman, H.L. (2019). Final analyses of OPTiM: a randomized phase III trial of talimogene laherparepvec versus granulocyte-macrophage colony-stimulating factor in unresectable stage III-IV melanoma. J. Immunother. Cancer 7, 145.

11. Kramm, C.M., Chase, M., Herrlinger, U., Jacobs, A., Pechan, P.A., Rainov, N.G., Sena-Esteves, M., Aghi, M., Barnett, F.H., Chiocca, E.A., and Breakefield, X.O. (1997). Therapeutic efficiency and safety of a second-generation replication-conditional HSV1 vector for brain tumor gene therapy. Hum. Gene Ther. 8, 2057–2068.

12. Todo, T., Martuza, R.L., Rabkin, S.D., and Johnson, P.A. (2001). Oncolytic herpes simplex virus vector with enhanced MHC class I presentation and tumor cell killing. Proc. Natl. Acad. Sci. USA 98, 6396–6401.

13. Mohr, I., Sternberg, D., Ward, S., Leib, D., Mulvey, M., and Gluzman, Y. (2001). A herpes simplex virus type 1 gamma34.5 second-site suppressor mutant that exhibits enhanced growth in cultured glioblastoma cells is severely attenuated in animals. J. Virol. 75, 5189–5196.

14. Kambara, H., Okano, H., Chiocca, E.A., and Saeki, Y. (2005). An oncolytic HSV-1 mutant expressing ICP34.5 under control of a nestin promoter increases survival of animals even when symptomatic from a brain tumor. Cancer Res. 65, 2832–2839.

15. Zhou, G., and Roizman, B. (2006). Construction and properties of a herpes simplex virus 1 designed to enter cells solely via the IL-13alpha2 receptor. Proc. Natl. Acad. Sci. USA 103, 5508–5513.

16. Montgomery, R.I., Warner, M.S., Lum, B.J., and Spear, P.G. (1996). Herpes simplex virus-1 entry into cells mediated by a novel member of the TNF/NGF receptor family. Cell 87, 427–436.

17. Geraghty, R.J., Krummenacher, C., Cohen, G.H., Eisenberg, R.J., and Spear, P.G. (1998). Entry of alphaherpesviruses mediated by poliovirus receptor-related protein 1 and poliovirus receptor. Science 280, 1618–1620.

18. Shukla, D., Liu, J., Blaiklock, P., Shworak, N.W., Bai, X., Esko, J.D., Cohen, G.H., Eisenberg, R.J., Rosenberg, R.D., and Spear, P.G. (1999). A novel role for 3-O-sulfated heparan sulfate in herpes simplex virus 1 entry. Cell 99, 13–22.

19. Menotti, L., Cerretani, A., and Campadelli-Fiume, G. (2006). A herpes simplex virus recombinant that exhibits a single-chain antibody to HER2/neu enters cells through the mammary tumor receptor, independently of the gD receptors. J. Virol. 80, 5531–5539.

20. Yoon, M., Zago, A., Shukla, D., and Spear, P.G. (2003). Mutations in the N termini of herpes simplex virus type 1 and 2 gDs alter functional interactions with the entry/fusion receptors HVEM, nectin-2, and 3-O-sulfated heparan sulfate but not with nectin-1. J. Virol. 77, 9221–9231.

21. Uchida, H., Marzulli, M., Nakano, K., Goins, W.F., Chan, J., Hong, C.S., Mazzacurati, L., Yoo, J.Y., Haseley, A., Nakashima, H., et al. (2013). Effective treatment of an orthotopic xenograft model of human glioblastoma using an EGFR-retargeted oncolytic herpes simplex virus. Mol. Ther. 21, 561–569.

22. Shibata, T., Uchida, H., Shiroyama, T., Okubo, Y., Suzuki, T., Ikeda, H., Yamaguchi, M., Miyagawa, Y., Fukuhara, T., Cohen, J.B., et al. (2016). Development of an oncolytic HSV vector fully retargeted specifically to cellular EpCAM for virus entry and cell-to-cell spread. Gene Ther. 23, 479–488.

23. Uchida, H., Chan, J., Goins, W.F., Grandi, P., Kumagai, I., Cohen, J.B., and Glorioso, J.C. (2010). A double mutation in glycoprotein gB compensates for ineffective gD-dependent initiation of herpes simplex virus type 1 infection. J. Virol. 84, 12200–12209.

24. Okubo, Y., Uchida, H., Wakata, A., Suzuki, T., Shibata, T., Ikeda, H., Yamaguchi, M., Cohen, J.B., Glorioso, J.C., Tagaya, M., et al. (2016). Syncytial Mutations Do Not Impair the Specificity of Entry and Spread of a Glycoprotein D Receptor-Retargeted Herpes Simplex Virus. J. Virol. 90, 11096–11105.

25. Bzik, D.J., Fox, B.A., DeLuca, N.A., and Person, S. (1984). Nucleotide sequence of a region of the herpes simplex virus type 1 gB glycoprotein gene: mutations affecting rate of virus entry and cell fusion. Virology 137, 185–190.

26. Debroy, C., Pederson, N., and Person, S. (1985). Nucleotide sequence of a herpes simplex virus type 1 gene that causes cell fusion. Virology *145*, 36–48.

27. Fu, X., and Zhang, X. (2002). Potent systemic antitumor activity from an oncolytic herpes simplex virus of syncytial phenotype. Cancer Res. *62*, 2306–2312.

28. Israyelyan, A.H., Melancon, J.M., Lomax, L.G., Sehgal, I., Leuschner, C., Kearney, M.T., Chouljenko, V.N., Baghian, A., and Kousoulas, K.G. (2007). Effective treatment of human breast tumor in a mouse xenograft model with herpes simplex virus type 1 specifying the NV1020 genomic deletion and the gBsyn3 syncytial mutation enabling high viral replication and spread in breast cancer cells. Hum. Gene Ther. *18*, 457–473.

29. Takaoka, H., Takahashi, G., Ogawa, F., Imai, T., Iwai, S., and Yura, Y. (2011). A novel fusogenic herpes simplex virus for oncolytic virotherapy of squamous cell carcinoma. Virol. J. *8*, 294.

30. Luo, Y., Lin, C., Ren, W., Ju, F., Xu, Z., Liu, H., Yu, Z., Chen, J., Zhang, J., Liu, P., et al. (2019). Intravenous Injections of a Rationally Selected Oncolytic Herpes Virus as a Potent Virotherapy for Hepatocellular Carcinoma. Mol. Ther. Oncolytics *15*, 153–165.

31. Liu, B.L., Robinson, M., Han, Z.Q., Branston, R.H., English, C., Reay, P., McGrath, Y., Thomas, S.K., Thornton, M., Bullock, P., et al. (2003). ICP34.5 deleted herpes simplex virus with enhanced oncolytic, immune stimulating, and anti-tumour properties. Gene Ther. *10*, 292–303.

32. Brown, S.M., Harland, J., MacLean, A.R., Podlech, J., and Clements, J.B. (1994). Cell type and cell state determine differential in vitro growth of non-neurovirulent ICP34.5-negative herpes simplex virus types 1 and 2. J. Gen. Virol. *75*, 2367–2377.

33. Jing, X., Cerveny, M., Yang, K., and He, B. (2004). Replication of herpes simplex virus 1 depends on the gamma 134.5 functions that facilitate virus response to interferon and egress in the different stages of productive infection. J. Virol. *78*, 7653–7666.

34. Speranza, M.C., Kasai, K., and Lawler, S.E. (2016). Preclinical Mouse Models for Analysis of the Therapeutic Potential of Engineered Oncolytic Herpes Viruses. ILAR J. *57*, 63–72.

35. Kaufman, H.L., Kohlhapp, F.J., and Zloza, A. (2015). Oncolytic viruses: a new class of immunotherapy drugs. Nat. Rev. Drug Discov. *14*, 642–662.

36. Russell, S.J., and Barber, G.N. (2018). Oncolytic Viruses as Antigen-Agnostic Cancer Vaccines. Cancer Cell *33*, 599–605.

37. Krabbe, T., and Altomonte, J. (2018). Fusogenic Viruses in Oncolytic Immunotherapy. Cancers (Basel) *10*, 216.

38. Fu, X., Tao, L., Jin, A., Vile, R., Brenner, M.K., and Zhang, X. (2003). Expression of a fusogenic membrane glycoprotein by an oncolytic herpes simplex virus potentiates the viral antitumor effect. Mol. Ther. *7*, 748–754.

39. Nakamori, M., Fu, X., Meng, F., Jin, A., Tao, L., Bast, R.C., Jr., and Zhang, X. (2003). Effective therapy of metastatic ovarian cancer with an oncolytic herpes simplex virus incorporating two membrane fusion mechanisms. Clin. Cancer Res. *9*, 2727–2733.

40. Simpson, G.R., Han, Z., Liu, B., Wang, Y., Campbell, G., and Coffin, R.S. (2006). Combination of a fusogenic glycoprotein, prodrug activation, and oncolytic herpes simplex virus for enhanced local tumor control. Cancer Res. *66*, 4835–4842.

41. Thomas, S., Kuncheria, L., Roulstone, V., Kyula, J.N., Mansfield, D., Bommareddy, P.K., Smith, H., Kaufman, H.L., Harrington, K.J., and Coffin, R.S. (2019). Development of a new fusion-enhanced oncolytic immunotherapy platform based on herpes simplex virus type 1. J. Immunother. Cancer *7*, 214.

42. O'Hara, B., Johann, S.V., Klinger, H.P., Blair, D.G., Rubinson, H., Dunn, K.J., Sass, P., Vitek, S.M., and Robins, T. (1990). Characterization of a human gene conferring sensitivity to infection by gibbon ape leukemia virus. Cell Growth Differ. *1*, 119–127.

43. Johann, S.V., Gibbons, J.J., and O'Hara, B. (1992). GLVR1, a receptor for gibbon ape leukemia virus, is homologous to a phosphate permease of Neurospora crassa and is expressed at high levels in the brain and thymus. J. Virol. *66*, 1635–1640.

44. Johann, S.V., van Zeijl, M., Cekleniak, J., and O'Hara, B. (1993). Definition of a domain of GLVR1 which is necessary for infection by gibbon ape leukemia virus and which is highly polymorphic between species. J. Virol. *67*, 6733–6736.

45. Tailor, C.S., Takeuchi, Y., O'Hara, B., Johann, S.V., Weiss, R.A., and Collins, M.K. (1993). Mutation of amino acids within the gibbon ape leukemia virus (GALV) receptor differentially affects feline leukemia virus subgroup B, simian sarcoma-associated virus, and GALV infections. J. Virol. *67*, 6737–6741.

46. Gierasch, W.W., Zimmerman, D.L., Ward, S.L., Vanheyningen, T.K., Romine, J.D., and Leib, D.A. (2006). Construction and characterization of bacterial artificial chromosomes containing HSV-1 strains 17 and KOS. J. Virol. Methods *135*, 197–206.

47. Tischer, B.K., von Einem, J., Kaufer, B., and Osterrieder, N. (2006). Two-step red-mediated recombination for versatile high-efficiency markerless DNA manipulation in Escherichia coli. Biotechniques *40*, 191–197.

48. Miyagawa, Y., Marino, P., Verlengia, G., Uchida, H., Goins, W.F., Yokota, S., Geller, D.A., Yoshida, O., Mester, J., Cohen, J.B., and Glorioso, J.C. (2015). Herpes simplex viral-vector design for efficient transduction of nonneuronal cells without cytotoxicity. Proc. Natl. Acad. Sci. USA *112*, E1632–E1641.

49. Uchida, H., Chan, J., Shrivastava, I., Reinhart, B., Grandi, P., Glorioso, J.C., and Cohen, J.B. (2013). Novel mutations in gB and gH circumvent the requirement for known gD Receptors in herpes simplex virus 1 entry and cell-to-cell spread. J. Virol. *87*, 1430–1442.

50. Uchida, H., Shah, W.A., Ozuer, A., Frampton, A.R., Jr., Goins, W.F., Grandi, P., Cohen, J.B., and Glorioso, J.C. (2009). Generation of herpesvirus entry mediator (HVEM)-restricted herpes simplex virus type 1 mutant viruses: resistance of HVEM-expressing cells and identification of mutations that rescue nectin-1 recognition. J. Virol. *83*, 2951–2961.